JOURNAL OF GEOPHYSICAL RESEARCH, VOL. 103, NO. A4, PAGES 7027–7041, APRIL 1, 1998

Electrostatic broadband ELF wave emission by Alfvén wave breaking

C. E. Seyler, A. E. Clark, and J. Bonnell[1]

School of Electrical Engineering, Cornell University, Ithaca, New York

J.-E. Wahlund

Swedish Institute of Space Physics, Kiruna

Abstract. The linear and nonlinear kinetic properties of electrostatic oblique waves below the lower hybrid frequency are investigated. For propagation angles $\vartheta = k_{||}/k_{\perp} < \sqrt{m_e/m_i}$ the waves are damped by either parallel electron Landau or ion cyclotron damping. For $T_i/T_e \gg 1$ the waves are only weakly damped and can propagate. These waves are called slow ion cyclotron (SIC) and slow ion acoustic (SIA) waves. A fluid-kinetic model, comprised of hot linear kinetic ions and cold nonlinear fluid electrons, is proposed to describe a nonlinear wave breaking process of small-scale Alfvén waves resulting in broadband extremely low-frequency (ELF) wave emission. Numerical solutions of the fluid-kinetic model are compared to the electric and magnetic fields of solitary kinetic Alfvén waves and broadband ELF waves observed by the Freja satellite within a hot ion environment. The agreement in waveform morphology and amplitude between the fluid-kinetic simulations and the observed waves provides support for the theory that observed SIA waves are the result of a nonlinear emission process from SIC waves.

1. Introduction

Small transverse scale Alfvén waves having dimensions in the range of 100 m to ~1 km, referred to as solitary kinetic Alfvén waves (SKAW), are commonly found in the topside ionosphere [*Wahlund et al.*, 1994; *Louarn et al.*, 1994; *Seyler et al.*, 1995; *Volwerk et al.*, 1996; *Seyler and Wahlund*, 1996] The transverse scale size of SKAW is comparable to the collisionless skin depth (or electron inertial length), and consequently, they are inertial Alfvén waves [*Seyler*, 1990; *Lysak*, 1991]. The electromagnetic characteristics of SKAW are significant for the larger scales of the order of a kilometer [*Seyler et al.*, 1995] but are not essential to their existence nor are they significant on scales of the order of a few hundred meters [*Seyler and Wahlund*, 1996]. In the electrostatic limit ($k_{\perp}c/\omega_p \gg 1$), SKAW have been called slow ion cyclotron (SIC) waves, terminology introduced by *Seyler and Wahlund* [1996] (hereinafter referred to as *SW*) to clarify their relationship to electrostatic ion cyclotron waves and to emphasize that for oblique propagation angles $\vartheta = k_{||}/k_{\perp} < \sqrt{m_e/m_i}$ the transverse phase velocity is slower than that of the electrostatic ion cyclotron wave (called the fast ion cyclotron (FIC) wave by *SW*). Alternate nomenclature has been introduced by *Lysak* [1997, this issue]. This class of waves was originally discussed by *Stringer* [1963]. *Stringer* [1963] called the FIC and SIC waves the ion cyclotron wave without making any distinction between propagation angles greater than or less than $\sqrt{m_e/m_i}$. The fast ion acoustic (FIA) and slow ion acoustic (SIA) waves of *SW* were collectively called the intermediate-frequency acoustic waves by *Stringer* [1963]. The additional fast and slow terminology is proposed to call attention to the very important differences in wave propagation characteristics for angles greater than and less than $\epsilon = \sqrt{m_e/m_i}$. An important distinguishing property between the fast and slow intermediate-frequency acoustic waves discussed by *SW* is the response of the plasma density to the electrostatic potential. It was shown that FIA waves have an electron Boltzmann response whereas SIA waves have an ion Boltzmann response. The ion Boltzmann response of SIA waves will be further clarified in this paper since it is a key property in identifying SIA waves within observational data.

Recent work by *Gekelman et al.* [1994, 1997], *Bellan* [1994] and *Stasiewicz et al.* [1997] suggests that the origin of SKAW may be due to inertial Alfvén resonance cones. The essential idea is the following: The dispersive behavior of inertial Alfvén waves produces a resonance cone at an angle from B_0 at which most of the wave energy propagates when emitted from a distant localized Alfvén wave source. Presumably, the location of

[1]Now at Los Alamos National Laboratory, Los Alamos, New Mexico.

Paper number 97JA02297.
0148-0227/97/97JA-02297$09.00

the Alfvén wave source is sufficiently far above the ionosphere so that the waves are localized by the time they reach the topside ionosphere. The cone angle is approximately given by $\epsilon\omega/\Omega_i$ for $\omega \ll \Omega_i$ [*Morales et al.*, 1994]. There is an annular region in the plane cut transverse to B_0 through which most of the Poynting flux propagates. This annular region has an approximate width of several collisionless skin depths $\lambda = c/\omega_{pe}$. The radius of the annulus widens with distance from the source. It should be clear that if the source is a line and not a point, then the cone simply becomes an angle.

Inertial Alfvén waves propagating within the resonance cone have a cone of constant phase with approximately the same angle as the resonance cone. This cone moves along B_0 at the Alfvén speed, so that a point of constant phase has a projected phase velocity in the transverse direction of approximately ϑv_A. Recall that $\vartheta = k_z/k_x$ is the angle of the wavevector with respect to the plane transverse to B_0. Therefore, waves within the resonance cone propagate nearly perpendicularly to the geomagnetic field. If a transverse cut is taken (along x) at a fixed distance along B_0 (fixed z), it would appear as though the waves start at the outer edge of the cone annulus, grow as they reach the center of the cone annulus, and decay as they approach the inner edge of the cone annulus. The origin of the localized constant frequency source is unclear, but at least one possibility comes to mind. It may be the same process that causes flickering aurora, which is believed to be caused by electromagnetic ion cyclotron waves [*Temerin et al.*, 1986] possibly excited by an electron beam [*Temerin and Lysak*, 1984].

The Alfvén resonance cone concept nicely explains the localized nature of SKAW, which is difficult to explain in any other fashion. Dispersive spreading seems to preclude SKAW as localized structures emitted from a moving zero-frequency disturbance (Alfvén wings), and it was shown by *Seyler et al.* [1995] that inertial Alfvén waves do not have nonlinear solitary wave solutions.

While the idea of an inertial Alfvén resonance cone may explain the concentration of Alfvén waves into a region of space comparable to the electron inertial length, this is a prediction of linear theory and therefore cannot explain the nonlinear evolution and dynamics of inertial Alfvén waves. The work of *Seyler et al.* [1995] and *SW* were attempts to describe the nonlinear behavior of SKAW using fluid models. In comparison to selected SKAW events from the Freja satellite, *Seyler et al.* [1995] and *SW* provided support for the notion that large-amplitude inertial Alfvén waves steepen by advective nonlinearity within the topside ionosphere to produce waveform morphology similar to observed electric and magnetic fields. *SW* suggested that the nonlinear steepening of inertial Alfvén waves leads to the emission of oblique acoustic waves (SIA waves) having a transverse phase velocity less than the acoustic speed. It was conjectured that these ELF wave emissions or the actual emission process could lead to parallel electron acceleration and transverse ion acceleration.

There have been several recent papers on high-latitude small-scale auroral energization processes connected with broadband ELF wave activity in the topside ionosphere below an altitude of 2000 km. These studies were based on detailed measurements carried out mainly by the Freja satellite, but also supported by the SCIFER and AMICIST sounding rocket observations [e.g., *Bonnell et al.*, 1996; *Kintner et al.*, 1996; *Lynch et al.*, 1996]. The Freja observations showed that the most common and intensive events of transversely accelerated ions (TAI) were not associated with lower hybrid wave activity [*Kintner et al.*, 1992; *Eliasson et al.*, 1994] but were clearly related to broadband mainly electrostatic ELF wave activity well below the lower hybrid cutoff [*André et al.*, 1994; *Wahlund et al.*, 1997; *Erlandson et al.*, 1994; *Norqvist et al.*, 1996; *Crew et al.*, 1990]. It was found that such broadband ELF activity was clearly intensified within localized regions containing either small-scale inertial Alfvén waves [*Wahlund et al.*, 1994; *Louarn et al.*, 1994; *Seyler et al.*, 1995; *Volwerk et al.*, 1996; *Stasiewicz et al.*, 1997] or large-amplitude electric field structures [e.g., *Marklund et al.*, 1994]. The characteristics of these broadband ELF emissions have been discussed by *SW* and *Wahlund et al.* [1997]. There are also some indications that TAI intensity increases within inertial Alfvén wave regions [*Knudsen and Wahlund*, 1997], but this issue is still unclear [*André et al.*, 1994]. A more definitive analysis of Freja observations has revealed that SKAW are associated with small-scale suprathermal electron bursts (STEB) (e.g., J. E. Wahlund et al., Electron energization by small-scale Alfvén waves, submitted to *Journal of Geophysical Research*, 1997, hereinafter referred to as Wahlund et al., submitted manuscript, 1997). Taken all together, the weight of observational evidence supports the contention that small-scale inertial Alfvén waves and associated ELF waves play an important role in ion and electron energization in the topside auroral ionosphere.

The present paper extends the results based upon an electrostatic two-fluid model discussed by *SW* to include important ion kinetic effects. The nonlinear dynamical model for ELF waves described herein is called the fluid-kinetic model, and is based upon the motion of nonlinear parallel fluid electrons and linear transverse kinetic ions. The fluid-kinetic model describes the SIC and SIA waves studied by *SW* but, unlike *SW*, includes important ion kinetic dispersive effects. The ion kinetic modifications introduce cyclotron resonances at harmonics of the ion gyrofrequency. Ion cyclotron resonances play an important role in the nonlinear emission of SIA waves from SIC waves and may influence transverse ion heating and acceleration.

On the basis of the theory given by *SW*, ELF waves in

the frequency range 20–400 Hz were found by *Wahlund et al.* [1997] to correspond closely with the theoretical properties of the SIC and SIA waves. This observational support for the existence of SIC and SIA waves and their close correlation to suprathermal electron bursts (STEB) and transversely accelerated ions (TAI) motivates us to understand the kinetic theory of the waves. This investigation is also necessary to reinforce our contention that they contribute to auroral particle energization.

2. Linear Kinetic Theory of SIC and SIA Waves

We consider the linear kinetic dispersive properties of electrostatic oblique waves having frequencies much less than the electron cyclotron frequency and propagating at an angle to the x axis $\vartheta \equiv k_z/k_x \ll \sqrt{m_e/m_i}$, where the magnetic field is assumed to lie along the z axis. The appropriate plasma dielectric function is

$$\epsilon(k_x,\vartheta,\omega) = 1 + \frac{k_{De}^2}{k^2} W\Big(\frac{\omega}{\vartheta k_x v_e}\Big) + \frac{k_{Di}^2}{k^2}\Big[1 + \sum_{n=-\infty}^{\infty} \frac{\omega\Lambda_n}{\omega - n\Omega_i}\Big[W\Big(\frac{\omega - n\Omega_i}{\vartheta k_x v_i}\Big) - 1\Big]\Big] \quad (1)$$

where $\Lambda_n \equiv I_n(\beta)e^{-\beta}$, and $\beta = k_x^2\rho_i^2$. The W-function is the plasma dispersion function defined by *Ichimaru* [1973].

We evaluate the dispersion relation using parameters similar to those of the Freja observational data (discussed later). Figure 1 (top) shows a plot of the real part of the frequency versus the perpendicular wavenumber. Figure 1 (bottom) shows the imaginary parts of the frequency corresponding to the two lowest branches of Figure 1 (top). The dashed line is the SIA linear dispersion curve from the fluid model of *SW*.

There are several aspects of these dispersion results that have not been, to our knowledge, discussed before

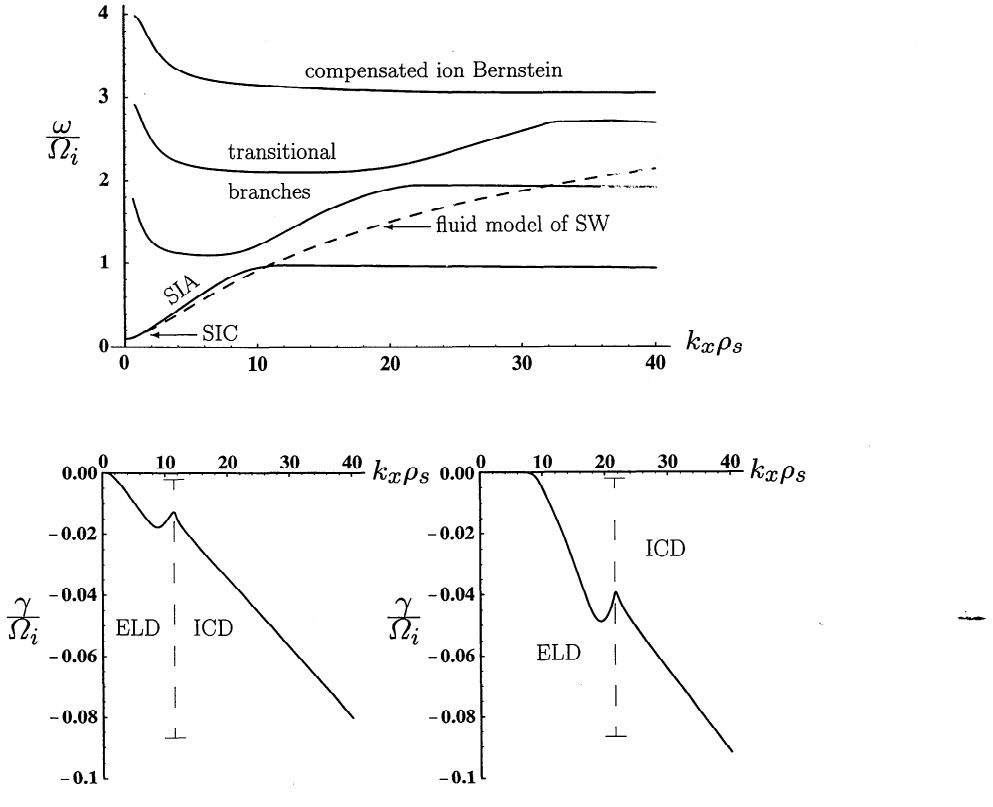

Figure 1. Plots of the linear mode frequency versus transverse wavenumber from (1). (top) The real part of the frequencies for four branches. The slow ion cyclotron (SIC) and slow ion acoustic (SIA) wave regions on the lowest branch are indicated. The transitional branches approximately track the two-fluid curve of *SW*. Above the ion plasma frequency cutoff lie the compensated ion Berstein modes. (bottom) The imaginary part of the frequencies for the lowest two branches. The transition from the electron Landau damping (ELD) dominated region to ion cyclotron damping (ICD) dominated region are indicated. The parameters are $\omega_{pi}/\Omega_i = 20$, $\theta \equiv \vartheta\sqrt{m_i/m_e} = 0.1$, and $T_i/T_e = 10$.

in the published literature. The behavior of the third and higher branches corresponds to the well-known compensated Bernstein modes which have nearly quasi-neutral character. The lowest branch agrees well for low wavenumbers with the fluid SIC wave, which is the flat portion of the curve near and below $k_x\rho_s = 1$, where $\rho_s = c_s/\Omega_i$. The SIC wave is the inertial Alfvén wave in the electrostatic limit ($k_x c/\omega_{pe} \gg 1$). The linear region of the lowest branch corresponds to the SIA wave. The fluid dispersion curve approaches the value $\vartheta\omega_{pi}$ asymptotically because of nonzero space charge effects, whereas the lowest kinetic branch asymptotes at the first cyclotron harmonic, yielding a resonance. This resonance is essential for ion cyclotron damping and transverse ion heating.

The lowest branch degenerates to zero frequency as the parallel wavenumber tends to zero. It is what we call the kinetic SIC/SIA branch. The kinetic properties of this branch have not been discussed to any discernible extent in the literature. Of particular interest is the region of maximum dispersion, which occurs near $k_x\rho_s = 1/\theta$, where $\theta \equiv \sqrt{m_i/m_e}\,\vartheta$ is the reduced angle discussed by *SW*. This is to be contrasted with the result in the fluid limit, where the SIA wave has maximum dispersion ($d^2\omega/dk^2$) at the Debye length scale. The kinetic dispersion scale becomes important when nonlinear steepening effects due to electron inertia are considered. Simulations will reveal that SIA wave emission from SIC waves occurs in this region of maximum dispersion.

The imaginary part of the frequency is due primarily to parallel electron Landau damping and secondarily to ion cyclotron damping for wavenumbers satisfying $k_x\rho_s < 1/\theta$. For larger wavenumbers, at and above the 'dispersive cusp', ion cyclotron damping dominates. The damping is not excessive for the temperature ratio chosen in this example (T_i/T_e=10), and it is likely that the waves would be of sufficient duration to be observed. Near $T_i/T_e \approx 1$ electron damping is considerably greater, and the waves would be damped significantly over one wave period. Ion cyclotron damping always dominates at large wavenumbers.

Lysak and Lotko [1996] investigated kinetic effects upon inertial Alfvén waves. They noted the important result that electron Landau damping decreases as the temperature ratio T_i/T_e increases even when the electron temperature remains constant. They point out that this is because higher ion temperature increases the wave phase velocity, thus moving the electron Landau resonance velocity further out on the tail of the electron distribution function. As noted by *SW*, a high T_i/T_e ratio is required in order that the slow acoustic waves not be strongly damped (a condition necessary for observability).

Lysak [1997, this issue] comments on alternate nomenclature for SIC and SIA waves, and their connection with inertial Alfvén waves in the electrostatic limit. The solutions of the kinetic dispersion relation for $\theta > 1$, which include the electrostatic ion cyclotron wave and the ion Bernstein modes, are also given in *Lysak* [1997], as are the algebraic derivations of the electrostatic fluid dispersion relations of *SW* for $\theta > 1$ and $\theta < 1$ from the kinetic dispersion relation in various fluid limits.

Figure 2 (solid curve) shows the ratio of the ion density perturbation δn_i to the potential $\delta\phi$, where the potential is normalized to T/e (T is the total temperature). This result shows ion polarization behavior ($\delta n_i \approx -n_0 k_x^2 \delta\phi/(B_0\Omega_i)$) for $k_x\rho_s < 1$, characteristic of Alfvén or SIC waves, and ion Boltzmann behavior ($\delta n_i \approx -e\delta\phi/T_i$) for wavenumbers in the range $1 < k_x\rho_s < 1/\theta$, characteristic of SIA waves. The kinetic results confirm the fluid analysis by *SW* of the ion Boltzmann response for wavenumbers satisfying $k_x\rho_s < 1/\theta$. It is important to note that if an electron Boltzmann response is assumed, then the lowest branch does not exist.

It should also be noted that the appropriate manner in which to display the dispersive behavior of this mode is at a fixed propagation angle (i.e., ω versus k) and not ω versus $k_\perp$ for a fixed $k_\parallel$ or vice versa. The last point emphasizes that these waves propagate in a direction nearly perpendicular to the magnetic field, and that the parallel and perpendicular phase velocities are projections of the phase velocity along **k** onto the z and

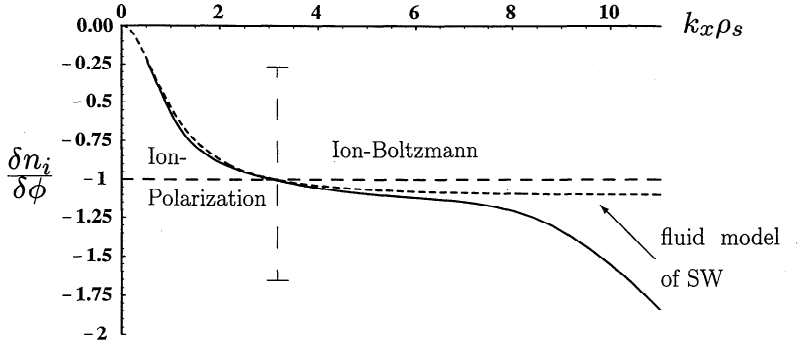

Figure 2. Plot of the ratio of the ion density to the electric potential. The result shows ion polarization response for wavenumbers in the range $k_x\rho_s < 1$ and an ion Boltzmann response in the range $1 < k_x\rho_s < 1/\theta = 10$. The approximate transition wavenumber from ion polarization to ion Boltzmann behavior is indicated.

x axes, respectively. The phase fronts of oblique waves progress in the direction of the nearly perpendicular wavenumber.

3. The Fluid-Kinetic Model

The development of the fluid-kinetic model proceeds by relating the ion fluid velocity to the perturbation electric field using the perturbation distribution function. We can derive a relatively simple and explicit linear time-dependent description for the ions if we only consider perpendicular ion motion and neglect parallel ion motion. This assumption is equivalent to neglecting ion cyclotron and Landau damping but retaining the ion cyclotron resonances. It is not possible to obtain such a simple formulation if the ions are nonlinear. We now outline the essential argument that justifies a linear ion treatment.

Slow ion cyclotron and slow ion acoustic waves are essentially quasineutral. Quasineutrality is maintained as a balance between transverse ion current and parallel electron current. The angle of propagation of SIA waves (ϑ) is less than $\epsilon \equiv \sqrt{m_e/m_i}$, which implies that the parallel electron fluid velocity exceeds ϵ^{-1} times the transverse ion fluid velocity. This fact together with an examination of the advective nonlinear terms in the fluid model reveals that the parallel electron advective nonlinearity is dominant over the transverse ion advective nonlinearity by the factor $1/\theta$, where θ is the reduced angle defined previously. Thus, if the electrons can be adequately modeled as a nonlinear fluid and if the ion motion is linear and transversely kinetic, then we arrive at a model that is of comparable complexity to the two-fluid description but which retains the essential ion dispersive effects that yield resonances at the cyclotron harmonics. It was determined by *SW*, through numerical experimentation and by comparing results with and without ion nonlinearity, that the effect of ion nonlinearity is weak for SIC and SIA waves.

The equations for ion motion in the fluid-kinetic model are found from the first moment of the perturbed distribution function. This calculation is given by *Swanson* [1989, 153pp.]. We define the fluid velocity for cyclotron harmonic n as

$$\hat{u}_{xn}(k_x,\omega) = -\frac{e}{m_i}\left[\frac{\Gamma_n(\beta)}{\omega^2 - n^2\Omega_i^2}\right] i\omega\hat{E}_x(k_x,\omega) \qquad (2)$$

where

$$\hat{u}_{ix} \equiv \sum_{n=1}^{\infty} \hat{u}_{xn} \qquad (3)$$

is the total perpendicular ion fluid velocity and $\Gamma_n(\beta) = 2n^2\Lambda_n(\beta)/\beta$.

If we multiply (2) by $n^2\Omega_i^2 - \omega^2$ and then inverse Fourier transform in time, we obtain a second-order equation for u_{xn} which can be expressed as two first-order differential equations for the dependent variables u_{xn} and u_{yn}. The kinetic ion model thus consists of the following equations:

$$\frac{\partial u_{xn}}{\partial t} = \frac{e}{m_i}\Gamma_n E_x + n\Omega_i\, u_{yn} \qquad (4)$$

$$\frac{\partial u_{yn}}{\partial t} = -n\Omega_i\, u_{xn} \qquad (5)$$

where the unhatted variables are the inverse temporal Fourier transforms of the hatted variables and it is understood that u_{xn} and u_{yn} are functions of k_x and t.

The variables u_{xn} and u_{yn} have a physical interpretation as the x- and y-components of ion velocity having a natural frequency response or resonance at the nth cyclotron harmonic. The harmonics are linearly coupled through the self-consistent electric field, and consequently, each cyclotron component of the ion flow velocity is driven at all cyclotron harmonics. The linear superposition of all harmonics constitutes the total ion fluid velocity. It is to be emphasized that the following equations are an exact mathematical consequence of linear transverse kinetic ions. The physical interpretation that we have offered has not entered into the derivation.

The system of equations is completed by the parallel electron fluid equations and the equation for the electric field which relates transverse displacement current and particle currents. These equations are

$$\frac{\partial n_e}{\partial t} + \vartheta\frac{\partial}{\partial x}(n_e u_{ez}) = 0 \qquad (6)$$

$$\frac{\partial u_{ez}}{\partial t} + \vartheta u_{ez}\frac{\partial u_{ez}}{\partial x} = -\frac{\vartheta e}{m_e}E_x - \frac{\vartheta T_e}{m_e n_e}\frac{\partial n_e}{\partial x} \qquad (7)$$

$$\frac{\partial E_x}{\partial t} = \frac{e}{\epsilon_0}(\vartheta n_e u_{ez} - n_0 u_{ix}) \qquad (8)$$

where n_0 is the background density.

The set of equations (3)–(8) comprise the fluid-kinetic model. The variables that are solved are the electron density n_e, the parallel electron velocity u_{ez}, the x-component of the electric field E_x, and the ion kinetic variables u_{xn} and u_{yn}. Equation (3) relates the ion kinetic variables to the total ion fluid velocity u_{ix}, which is used to determine the electric field in (8). A Fourier spectral method, very similar to that discussed by *SW*, is used to compute spatial derivatives and the ion kinetic term $\Gamma_n E_x$ in (4). This model is intended to be a more accurate nonlinear description of slow ion cyclotron and ion acoustic waves discussed in the two-fluid context by *SW*.

4. Simulations and Comparison to Freja Satellite Observations

We present results of simulations based upon the fluid-kinetic model and compare them to three selected events of SIC and SIA waves detected by the Freja

spacecraft. Two of the Freja ELF wave events have been discussed previously; we will refer to the appropriate papers for a more detailed discussion of those events. One event, not previously published, is very relevant to the simulation results and is discussed in this paper. We will present the simulation snapshots that display the characteristic signatures and features of the density, electric fields and magnetic fields associated with the SIC and SIA waves seen in the data.

The simulation magnetic field data are processed in such a manner as to simulate the search coil magnetometer (SCM) response. The Freja SCM has a frequency response that essentially measures the derivative of the transverse magnetic field (B_y in our geometry) for frequencies below ~30 Hz. The derivative of B_y is proportional to the parallel current density. Above 30 Hz the SCM measures the actual magnetic field. To model the SCM response, a one-pole filter of the form $ik/(ik + k_0)$ is applied to the spatial Fourier transform of B_y. This represents the simplest model having the necessary high-pass characteristics. The filter parameter k_0 is the wavenumber corresponding to the cutoff frequency (in rad s^{-1}) divided by the spacecraft velocity. A correct application of this SCM model assumes that the ELF waves are frozen during the Freja transit and that the transverse phase velocity of the waves is much less that the Freja velocity of 7 km s^{-1}.

All simulation results are derived from the fluid-kinetic equations (3)–(8) using periodic boundary conditions. The adjustable parameters in the simulation model are the reduced angle $\theta = \vartheta\sqrt{m_i/m_e}$, $\alpha = \omega_{pi}^2/\Omega_i^2$, and the amplitude of the sinusoidal initial condition corresponding to a slow ion cyclotron wave with a wavelength equal to the system length. The parameter ranges that were studied most extensively were the following: the reduced angle θ was varied between 0.02 and 0.2; α was varied between 100 and 1000, but the results were insensitive to α for values greater than ~100; the density perturbation amplitude was varied between 0.2 and 0.25; the temperature ratio T_i/T_e was chosen to be 10.

The results depend somewhat upon the number of cyclotron harmonics that were used (see the summation in (3)). Clearly, we have to limit the number of harmonics, but if we adhere to the constraints imposed by the justification of the model, more harmonics implies more accurate results. We found that above ~10 or so harmonics the results were essentially the same. This indicates that convergence was achieved in the number of harmonics. It was found, however, that some of the following comparisons to observational data were considerably better when a smaller number of harmonics were retained. We have no explanation for this result, but since justification of the model relies upon a large number of harmonics, we have presented only converged results involving a sufficiently large number of harmonics. The simulation results shown were generated using 40 harmonics.

Three simulation snapshots are presented, and all correspond to the following set of parameters: $\theta = 0.088$, $\alpha = 300$, and initial density amplitude $\delta n/n_0 = 0.22$. The only parameter that was varied between simulations was the SCM one-pole model parameter k_0 corresponding to the low pass frequency cutoff. Varying this parameter is equivalent to setting the scale size in meters. Since the simulation length is normalized to the acoustic gyroradius ρ_s, this is the same as assuming an ion temperature. There is only limited information about the temperatures for the observed events, so in practice we vary the simulated SCM cutoff frequency to achieve the best agreement with SCM data. The times of the snapshots were also selected for the best match to the data.

We have elected to present results from a single set of simulation parameters (except k_0) to emphasize that the results and their agreement with observations are not very sensitive to parameter selection. The fact that a single set of parameters produces different morphological features that are identified in different observed events supports the viability of the model. A very simple initial condition corresponding to a single slow cyclotron (inertial Alfvén) wave having an amplitude sufficient to result in wave breaking is sufficient to produce reasonable agreement with observations. We emphasize that all small-scale and higher-frequency waves which are emitted from this simple initial condition are the result of Alfvén wave breaking.

The most important variable was the time selected for comparison. All the simulations went through similar stages of evolution, each stage having distinct features in the waveforms. Comparison plots were selected on the basis of the best qualitative and quantitative agreement as determined by eye. We realize that such subjective comparisons are subject to bias and rely substantially upon morphological interpretation. We have, however, examined a large number of simulation runs depending upon different parameters and found that similar patterns arise. We emphasize that the present model produces results that bear some similarity to the fluid simulations of *Seyler et al.* [1995] and *SW*. There are, however, essential differences, some of which are only apparent upon scrutinization of details from many simulations. We have tried to present sufficient information about the model and parameters so that one could reproduce the results presented here if one were so inclined.

A slow ion cyclotron wave of modest amplitude is found to steepen nonlinearly into a SKAW. The term SKAW, used by *Wahlund et al.* [1994], is taken here to refer to a nonlinearly steepened inertial Alfvén wave or its electrostatic equivalent, the SIC wave. The steepening stage is characterized by a large negative electric field spike due to the ion Boltzmann potential response to the steep density gradient. Subsequently in time, the negative electric field spike is followed by a positive electric field spike. This ultimately results in

SIA wave emission, characterized by electric and magnetic field oscillations near and below the first cyclotron resonance and occurring on spatial scales near the ion sound gyroradius. In the latter stages of evolution it was often found that two or more small-scale density spikes emerged from a rather structureless density profile. Associated with these density spikes were electric field variations having a positive and negative swing on either side of the density spike consistent with an ion Boltzmann response. It was also found that these bipolar features would disappear and later reappear quasiperiodically for a long simulation of 200 Ω_i^{-1} or longer.

Data are shown from three simulations for which we have selected the time to achieve the best agreement with three selected events from the Freja spacecraft. We will focus on the Freja F4 electric field, density and SCM data. These data are from orbit 3183, which was an event discussed by *Seyler et al.* [1995], orbit 6838, which was discussed by *SW*, and orbit 1550, which has not been presented elsewhere. We will discuss the event of orbit 1550 last. For the purpose of comparing the dimensionless simulation electric and magnetic field amplitudes to data we assume nominal Freja conditions ($c_s = 8$ km s^{-1}, $B_0 = 2.5\times10^{-5}$ T, and $n_0 = 10^9$ m^{-3}). This corresponds to one unit of electric field equal to $c_s B_0 = 200$ mV m^{-1} and one unit of magnetic field equal to $B_0(c_s^2/v_A^2)\sqrt{m_i/m_e} = 16$ nT [*SW*]. One should not use these values too literally for comparison purposes since the ion and electron temperatures can vary appreciably from event to event and we do not have reliable values of these for any event. For this reason we choose to display simulation data in normalized units.

We have reversed the x-axis in all three simulation snapshots to compare more favorably with the waveform morphology seen in the data. Since the initial SIC wave is launched to the right, this implies that the observed events by Freja were head-on encounters of SKAW. It is very important to realize that in reversing the x-axis the sense of the electric field with repect to density gradients is also reversed. This means that an ion Boltzmann electric field response would appear as a negative response to a positive density gradient. This should not be confused with an electron Boltzmann response.

Figure 3 is a SKAW event from Freja orbit 3183 which was discussed by *Seyler et al.* [1995] and compared to a fluid simulation. It was noted that the electric antenna was close to parallel, so that the actual electric field is probably considerably larger than indicated on the plot. There was no density information available for this event. Figure 4 shows the (a) density, (b) electric field, and (c) SCM response ($k_0 = 3$) from a fluid-kinetic simulation intended for comparison to the event of orbit 3183 shown in Figure 3. This snapshot is representative of the steepening stage. The feature of this result that compares well to the data is the ion Boltzmann negative electric field spike associated with the

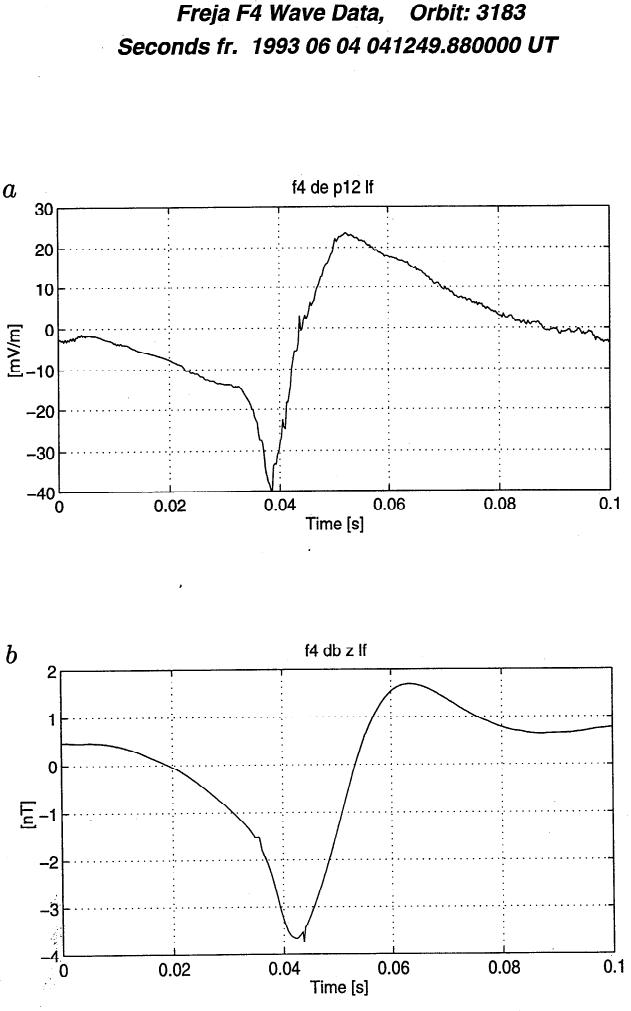

Figure 3. The electric field and search coil magnetometer (SCM) field for an event on orbit 3183 discussed by *Seyler et al.* [1995]. Note the prominent electric field spike which is interpreted to be the ion Boltzmann response to a steepened density profile. Density information was not available for this event.

steepened density profile. The detailed shape of the electric field is in agreement with the observed electric field. Since the antenna is close to parallel, appreciable attenuation of the measured electric field amplitude is introduced. We can, however, provide a test of the reasonableness of the simulation amplitude by estimating what the acoustic speed would have to be in order for the electric fields to agree. If the displayed value of the peak electric field amplitude of 40 mV m^{-1} is used, this implies an acoustic speed of $c_s = 2$ km s^{-1}, a value that is almost certainly too low. If, instead, a measured electric field of 200 mV m^{-1} is taken, corresponding to an antenna angle of 75°–80° off perpendicular, this yields a value of $c_s = 10$ km s^{-1} which is a more reasonable estimate. Thus the simulation electric field amplitude is consistent with the estimated observed value. The two-fluid model also agrees well with the characteristic features of this event [*Seyler et al.*, 1995]. The simulated SCM waveform agrees fairly well with the data

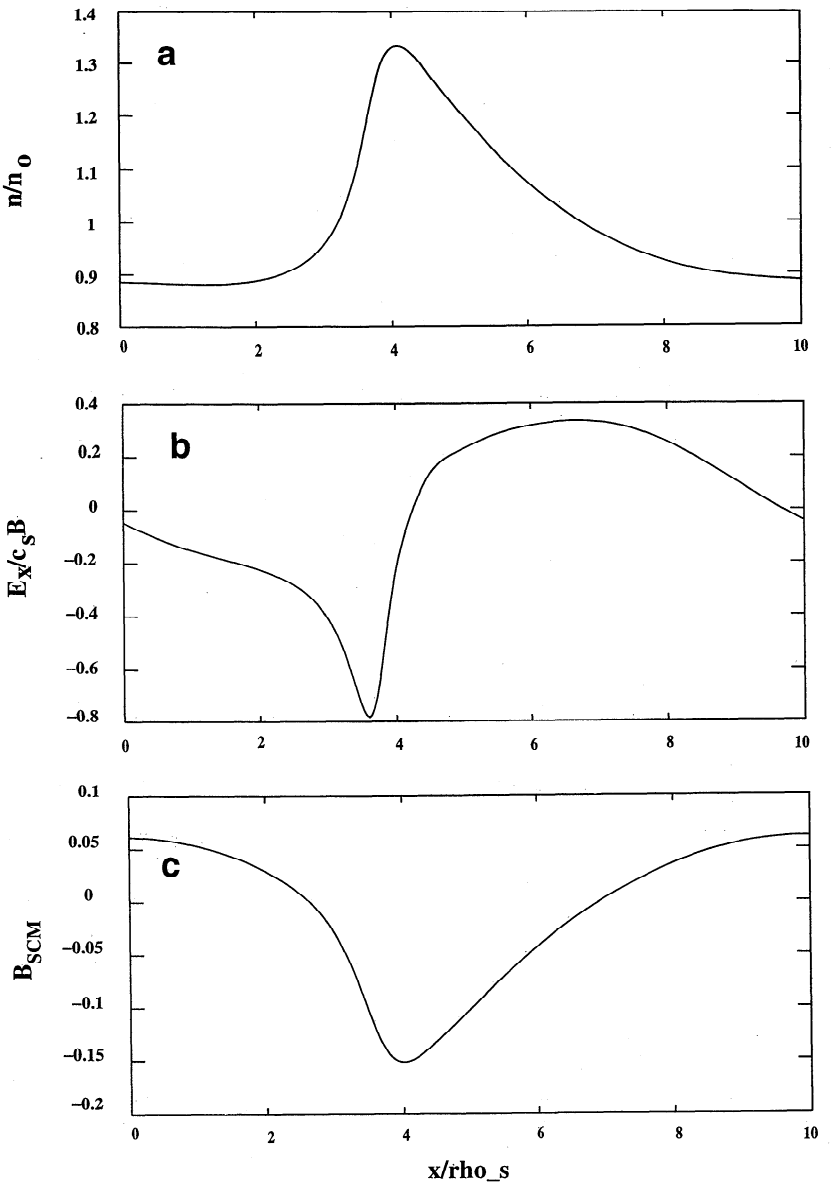

Figure 4. The (a) density, (b) electric field and (c) simulated SCM field for a fluid-kinetic simulation corresponding to the steepening phase of a SIC wave. This run is intended for comparison to Figure 3. The parameters for the run are $\theta = 0.088$, $\alpha = 300$, $\delta n/n = 0.22$ (the initial amplitude of the sinusoidal SIC wave), and $k_0 = 1.0$ is the SCM high-pass cutoff parameter. The snapshots correspond to time 31 Ω_i^{-1}. The plotted electric field is normalized as $\widetilde{E} = E/c_s B_0$.

except that perhaps there is some bipolar character in the data that is not apparent in the simulation. To compare the SCM amplitudes, use $v_A = 3 \times 10^3$ km s^{-1} for O^+ and $c_s = 10$ km s^{-1} to find, using the formula above, $B \approx 7$ nT. This compares reasonably well to the observed 4 nT when the uncertainties of measurement are taken into consideration.

The (a) density, (b) electric field and (c) SCM ($k_0 = 1.0$) results from the event of orbit 6838 are shown in Figure 5. This event was previously discussed by *SW* as a possible example of SIA soliton emission from a larger-scale SIC wave and is known to be associated with hot ions. See the discussion by *SW*. We believe this interpretation still holds with some slight modifications. The large-scale SIC wave corresponds to the density enhancement and large magnetic perturbation centered around time 0.04 s. To the right of the main SKAW are two smaller density peaks (time between 0.06 and 0.09 s) and about three cycles of electric field oscillation. The electric field oscillations exhibit an approximate ion Boltzmann response to the two density enhancements. There is also a small but easily detectable magnetic perturbation associated with the electric field fluctuations of about 0.3 nT.

Figure 6 displays the results of a simulation snapshot that is comparable to the event of orbit 6838. The main features to be compared to data are the density spikes and the associated electric field oscillations seen in Fig-

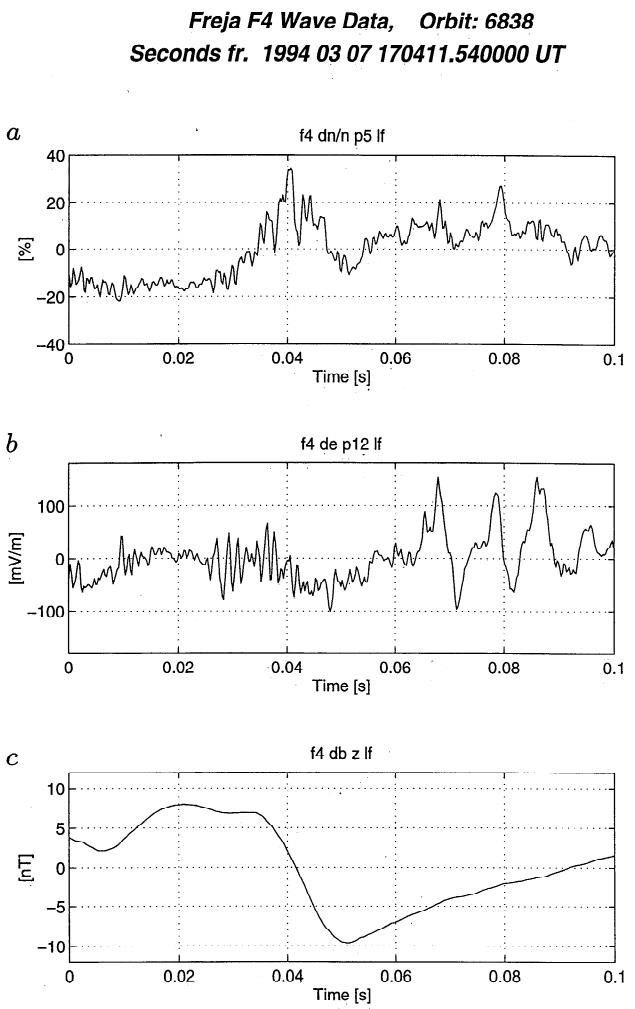

Figure 5. The (b) electric field and (c) SCM field for an event on orbit 6838 discussed by *Seyler et al.* [1995]. Note the two ion Boltzmann density spikes (a) which are correlated with the large-amplitude electric field oscillations. There are also small-amplitude magnetic field perturbations which are correlated with the electric field oscillations.

ures 6a and 6b, respectively. The main difference between the simulation and the data is that in the simulation the density spikes associated with the largest electric field oscillations are superimposed on the density perturbation associated with the large-scale SIC wave. The data show significant separation between what we interpret to be the SIC density perturbation and the SIA density perturbation. It appears that the SIC wave has propagated ahead of the emitted SIA waves in the data but not in the simulation. This is perhaps due to the higher phase velocity of the SIC waves.

For amplitude comparison of the electric field we will again use the simulation and data to estimate the acoustic speed. A reasonable value of c_s then implies reasonable agreement of the amplitudes. Using a dimensionless electric field perturbation of 2.5 and a measured electric field of $\sim$250 mV m^{-1} we arrive at $c_s = 4$ km s^{-1}. This value is somewhat lower than we would expect, but not unreasonable. We suspect that the source of disagreement lies in the value of θ chosen for the simulation. A higher value of θ would result in a lower dimensionless electric field and a higher estimate of c_s. We have substantiated this from other simulations but still prefer to present the results of a single set of simulation parameters to compare to all actual events rather than to attempt to fit each event in detail.

As noted above, the emission of isolated SIA waves were found to reoccur quasiperiodically during a long fluid-kinetic simulation. These SIA wave emissions are reminiscent of the solitary waves discussed by *SW* and shown to be the primary form of wave emission for the two-fluid model. Solitary waves have a characteristic spatial scale associated with the linear dispersion scale length. The dispersive scale of the fluid-kinetic model is the region of largest negative curvature in the lowest branch of Figure 1, which is close to $\theta\rho_s$, whereas in the pure two-fluid model, the dispersive scale is the Debye length. Under reasonable Freja conditions the Debye length is of the order of a few tens of centimeters which is much smaller than the measured width of $\sim$15 m of the density spike located at 0.08 s. If ρ_s is estimated to be 70 m (0.1 s corresponding to the separation between the electric field oscillations), then the kinetic dispersion scale is of the order of 7 m if $\theta = 0.1$. Thus the fluid-kinetic model is in much better agreement than the two-fluid model in this respect.

Our third and final comparison is to an event from orbit 1550, which has not been reported before. The event of interest on orbit 1550 is shown in Figure 7 and centered around time 0.08 s. The prominent features of this event are a large negative electric field spike having an amplitude greater than 200 mV m^{-1} with oscillations trailing off to the right (Figure 7b), a large SCM response ($k_0 = 3.0$) which is correlated with the electric field spike, and the distinct trailing 50 Hz oscillations which are correlated with subsequent electric field oscillations (Figure 7b). The small-scale density perturbations shown in Figure 7a are somewhat erratic but are easily detectable. They are correlated with the electric field in an ion Boltzmann manner. The correlation of the electric field with the SCM oscillations are probably due to parallel electron currents produced by the parallel component of the electric field. This event occurred in hot ion conditions as determined by F3H instrument data (P. Norqvist, private communication, 1995).

Figure 8 presents the (a) density, (b) electric field, and (c) simulated SCM results from the same simulation as shown in Figure 6 but at a later time. This snapshot was selected to show the slow acoustic wave oscillations in the SCM data. The trailing oscillations correspond to the first cyclotron resonance of the kinetic SIA branch (refer to Figure 1) as determined by examination of a series of sequential snapshots and calculation of the phase velocity. The electric field exhibits

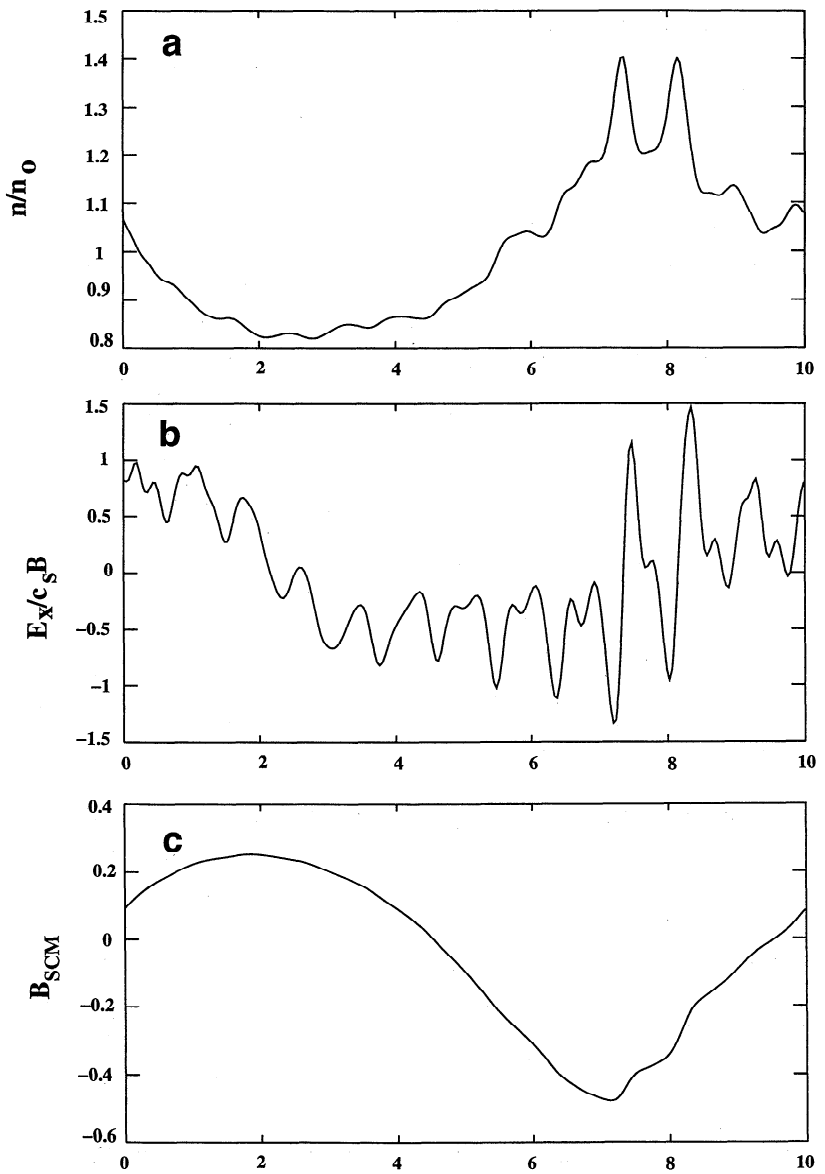

Figure 6. A fluid-kinetic simulation snapshot of the (a) density, (b) electric field and (c) simulated SCM field intended for comparison to Figure 5. The parameters for the run are the same as those for Figure 4. The snapshot corresponds to time 250 Ω_i^{-1}, and displays two ion Boltzmann density spikes and corresponding electric field oscillations.

the large negative spike as well as cyclotron oscillations correlated with those of the simulated SCM waveform. The emitted short-scale SIA waves have a phase velocity that is close to, but somewhat less than, the initial SIC wave. Thus, these waves lie near the concave downward portion of the SIA branch of Figure 1 ($k_x\rho_s \approx 1/\theta$) and have an approximate phase velocity of θc_s.

This snapshot is intended for comparison to the event in orbit 1550, and the agreement would suggest that SIA waves are responsible for the distinctive SCM perturbations. As in the simulations, the SCM perturbations are correlated with the density and electric field oscillations. The agreement between the large-scale density perturbation in the simulation and the data does not appear to be very good. Where the simulation predicts a large-scale density enhancement, the data show a density depletion. This discrepancy was also noted in the two-fluid model and compared to other Freja events by *Seyler et al.* [1995]. We will offer an explanation for the large-scale discrepancy in the δn comparison in section 5. We emphasize, however, that both the simulation and the data have small-scale density and electric field correlations that are consistent with an ion Boltzmann response.

All three simulation snapshots reveal small-scale structure that is produced by nonlinear steepening and a process similar to classical wave breaking. To show that this nonlinear mechanism produces broadband ELF

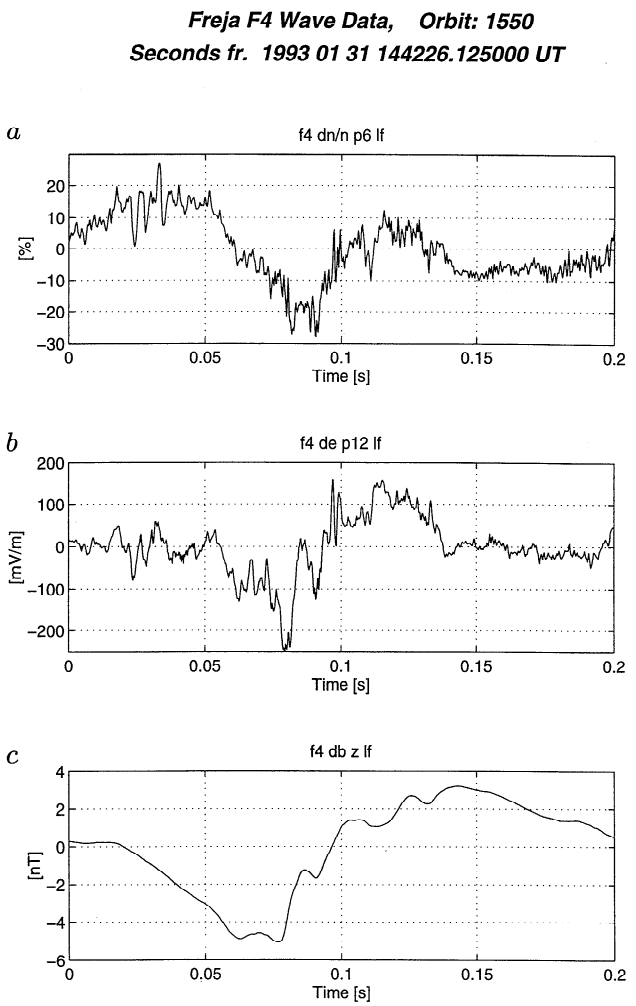

Figure 7. Freja spacecraft data from orbit 1550. Shown are the F4 (a) density, (b) electric field and (c) SCM waveforms. The event has distinctive oscillations in the SCM response correlated with small-scale electric field and density oscillations. Note that the large-scale density depletion is centered near the region of largest magnitude small-scale electric and magnetic field perturbations. The F3H hot ion energy analyzer indicated ion temperatures close to 30 eV for this event.

waves, we present a plot (Figure 9) of the temporal power spectrum of the electric field for the simulation around the time of Figure 8. Note that there is significant relative power in the waves emitted near the lower-lying cyclotron harmonics. Thus an initially monochromatic inertial Alfvén wave having a frequency well below the ion cyclotron frequency (25 Hz) emits a broadband spectrum of slow ion acoustic waves and higher-frequency compensated ion Bernstein waves up to several hundred hertz. A verification of the discrete spectral features associated with the nonlinear emission process is difficult to do experimentally because of the extreme Doppler broadening. It is clear, however, that large-amplitude SKAW are strongly correlated with broadband ELF emissions [*Wahlund et al.*, 1994; *Louarn et al.*, 1994; *Seyler et al.*, 1995, *SW*] We have presented one possible scenario for the origin of these waves that has significant observational support.

5. Discussion and Summary

It is our contention that the ELF wave events observed during orbits 3183, 1550, and 6838 are snapshots characteristic of short-scale Alfvén wave steepening and subsequent nonlinear emission of SIA waves in the topside ionosphere. A similar thesis was proposed based upon the results of the two-fluid simulations of *SW*. There are, however, three important differences between the two-fluid model and those of the fluid-kinetic model that provide further support for this scenario. These differences pertain to the dominant spatial scale at which emission occurs, the amplitude of the wave emissions, and the characteristic emission frequencies.

As discussed by *SW*, SIA wave emission occurs in the region of maximum dispersion. For the two-fluid model this corresponds to the Debye scale whereas for the fluid-kinetic model the wave emission occurs near $\theta\rho_s$. For the parameters $\theta = 0.1$ and $\omega_{pi}/\Omega_i = 20$ the emission scale for the fluid-kinetic model is larger than the Debye scale, which is in better agreement with observations. Note that $\sqrt{\alpha} = \omega_{pi}/\Omega_i = \rho_s/\lambda_D$ for equal ion and electron temperatures. For the typical Freja conditions stated previously this value is of the order of a hundred or more. Thus, for $\theta = 0.1$ the kinetic dispersion scale $\theta\rho_i$ is at least 10 times larger than the fluid dispersion scale λ_D.

The second important difference is that for the fluid-kinetic model the emitted wave amplitudes are much closer in agreement with the observations. The two-fluid model tends to emit waves with very large density and electric field perturbations. The two-fluid model predicts wave emission amplitudes that are several times larger than the fluid-kinetic model. Using the standard Freja parameters, typical simulation electric field emission amplitudes are in the range of 100–300 mV m^{-1} for the fluid-kinetic model, whereas they were often considerably larger for the two-fluid model.

The third difference is that emission power resides predominantly near the first few ion cyclotron harmonics for the fluid-kinetic model, whereas for the two-fluid model the emission process yields distinct solitary waves having a continuous power spectrum.

Two very important phenomena that are often correlated with SKAW are suprathermal electron bursts (STEB) and TAI. There is a strong observational correlation between specific STEB events and large-amplitude electric field and SCM measurements (Wahlund et al., submitted manuscript, 1997). So, it seems clear that some STEB are a consequence of the nonlinear steepening and wave acceleration process. *Hui and Seyler* [1992] have offered this suggestion on the basis of previous simulation results. Also, the emission of waves near the ion cyclotron resonances and the concentration of electric field power in the ion cyclotron har-

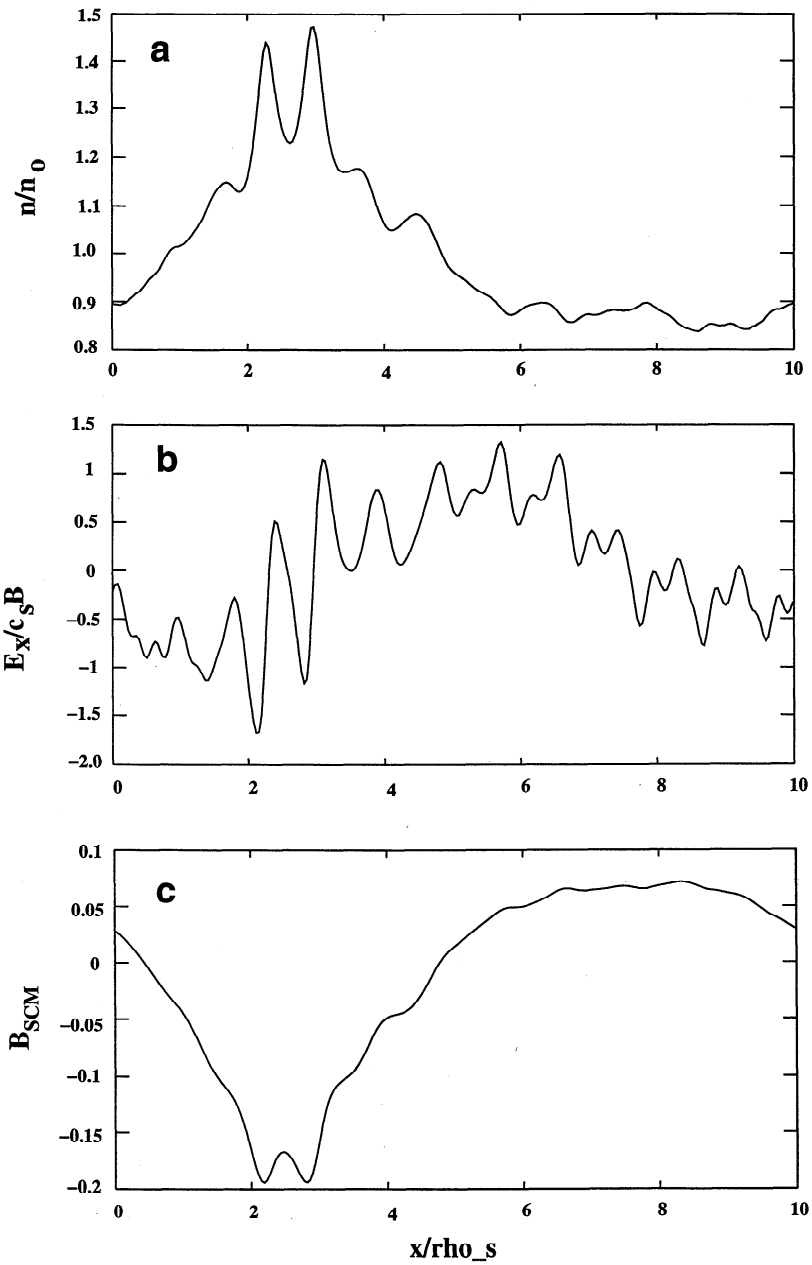

Figure 8. The (a) density, (b) electric field and (c) simulated SCM field for a fluid-kinetic simulation showing SIA wave emission from an SIC wave. The parameters for the run are the same as those in Figures 4 and 6, except that here the SCM high pass cutoff parameter is $k_0 = 3.0$. The snapshot corresponds to time 280 Ω_i^{-1} and is intended for comparison to the event in Figure 7. Note that the electric and SCM oscillations are correlated and display the gross features found in the data. The small-scale density perturbations are characteristic of an ion Boltzmann response and are consistent with small-scale density perturbations found in the data. The large-scale density is an enhancement which disagrees with the observed density depletion (Figure 7a).

monics would enhance the efficiency of ion cyclotron resonance heating relative to a continuous ELF wave spectrum. Although the present results do not verify that the SIA wave emission process leads to TAI, they do suggest that heating via the ion cyclotron resonance process is likely. The emission of SIA waves when the ions and electrons are nearly equal in temperature needs to be explored. In that case the SIA waves are strongly damped by electron Landau damping, although ion cyclotron damping still dominates at scales smaller than $\theta\rho_s$. If SIA emission occurs for equal temperatures, then the process may be consistent with ion heating as well

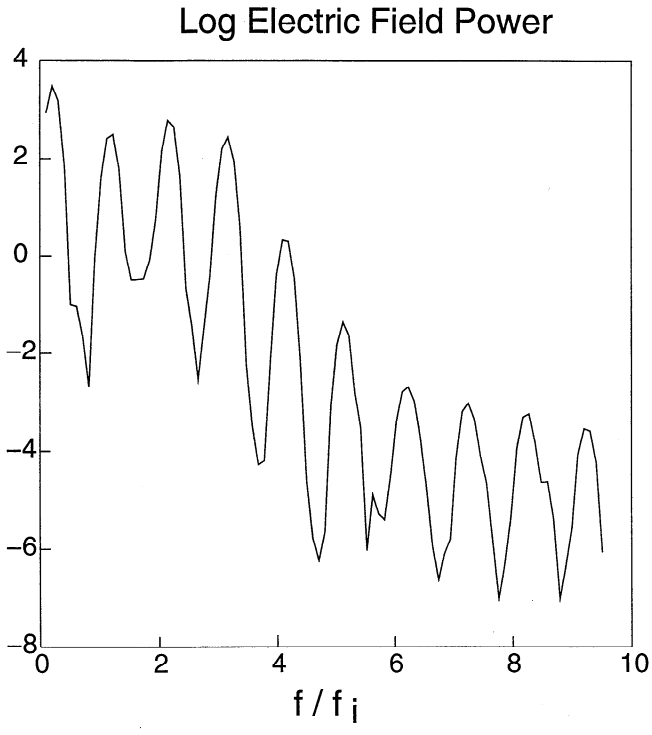

Figure 9. Plot of the temporal power spectrum of the electric field for the simulation around the time corresponding to Figure 6. Note that most of the relative power is in the waves emitted near the lower-lying cyclotron harmonics.

as STEB. The fluid-kinetic model cannot directly address the origin of the STEB or TAI since all resonant absorption of energy by particles has been neglected.

The stability of the one-dimensional solutions to perturbations in the y-direction was addressed in part by *Seyler* [1990], although the model used by *Seyler* [1990] did not include the important compressible nonlinear terms that lead to advective steepening and associated wave emission. It was found that the inertial Alfvén waves were marginally stable if the waves did not interfere with waves reflected from the ionosphere. For short-circuit voltage reflections the waves are unstable to a collisionless tearing-mode instability which destroys the sheet-like structure to produce current filaments. For open-circuit current reflections the inertial Alfvén wave is unstable to a Kelvin-Helmholtz instability which also breaks the longitudinal (y) invariance to produce curls and vortices. If SKAW have their origin in an Alfvén resonance cone, then it would seem that waves reflected from the ionosphere would not interfere with incident waves at Freja altitudes since the cone angle is likely to be sufficiently large to allow the reflected waves to miss the incident waves. For a cone angle of 0.001 and a transverse scale of 1 km the reflection point would need to be more than 1000 km from the altitude at which the SKAW is encountered. There is evidence, however, that SKAW do have two-dimensional structure at scales near ρ_i [*Volwerk et al.*, 1996], so that there may be reflection interference in some cases or possibly some other reason for two-dimensional SKAW breakup.

Finally, we comment on the discrepancy between the large-scale density perturbations found in the simulations and the observations. As we noted before, the agreement for small-scale density perturbations associated with the ion Boltzmann response of slow acoustic waves is good. We also pointed out that on scales comparable to the larger-scale inertial Alfvén waves the observations often indicated a depletion where the model predicted an enhancement. We believe that these density depressions are due the presence of the broadband ELF waves. Numerous SKAW examples exist in which a density depression is associated with SKAW, as was pointed out by *Stasiewicz et al.* [1997]. They contend that this is evidence for an Alfvén cavity resonator [*Trakhtengerts and Feldstein*, 1984; *Lysak*, 1991]. However, it is also the case that where density depressions occur broadband ELF wave activity is also found [*Wahlund et al.*, 1994; *Seyler et al.*, 1995, *SW*]. We suggest that it is the ELF waves that produce the density depression through the ponderomotive force [e.g. *Chen*, 1984]. The ponderomotive expulsion of plasma may explain the origin of the cavity as well as the discrepancy with the simulation results. This idea also fits well with the the concept that inertial Alfvén resonance cones are the source of SKAW. The continual flux of large-amplitude inertial Alfvén waves along a resonance cone trajectory and nonlinear wave breaking within the resonance cone layer implies concentrated ELF wave activity, accelerated ions, and ponderomotive expulsion of plasma. The one-dimensional fluid-kinetic model is not adequate to address this question. A two-dimensional (x-z) electromagnetic model will be necessary to investigate phenomena associated with inertial Alfvén resonance cones such as ponderomotive density cavity formation.

In summary, we have presented the linear kinetic theory for two classes of nearly perpendicular electrostatic waves originally discussed by *Stringer* [1963], the slow ion cyclotron and slow ion acoustic waves. We found that the lowest normal mode branch can be weakly damped at wavelengths greater than $\theta\rho_s$ when the ions are much hotter than the electrons. For these wavelengths the dispersion characteristics of the fluid model and the the lowest branch of the kinetic model were in good agreement. The ion polarization response of the SIC wave and the ion Boltzmann response of the SIA wave were also confirmed by the kinetic model for wavelengths at which damping is small. We proposed a fluid-kinetic model having undamped linear ion kinetic dynamics and nonlinear fluid electron dynamics to describe the SIC and SIA waves. This model predicts that large-amplitude SIC waves will steepen and subsequently emit SIA waves. This emission process is characterized by several distinct features that are often found in Freja satellite observations of ELF waves when hot ions are present.

A comparison of the results of fluid-kinetic simulations to Freja observations of ELF waves provided what we believe to be compelling evidence that the observed slow ion acoustic waves were the result of a nonlinear emission process from inertial Alfvén waves (SIC waves). We speculated that large negative electric field spikes produced by the SIA wave emission would be accompanied by bursts of accelerated electrons (STEB). The presence of significant relative power in the cyclotron harmonics of SIA waves as computed from the fluid-kinetic simulations lead us also to speculate that ions could be transversely accelerated by resonant absorption. These speculations about the production of STEB and TAI may be addressed using a particle-in-cell (PIC) model of the waves we have considered here. We are currently investigating electron and ion energization using a completely kinetic PIC model, and we will report on the results in a future publication.

The present model is one-dimensional and as such cannot address issues regarding the possible origin of SKAW, inertial Alfvén cavity resonators associated with SKAW, and ponderomotive formation of density cavities. The results of one-dimensional model comparisons to Freja observations are consistent, however, with the idead that inertial Alfvén resonance cones are possible sources for SKAW. A more comprehensive model should include ion kinetics, electromagnetic effects, and electron nonlinearity. Work on such a model is in progress.

Acknowledgments. The work of C. E. S. and A. E. C. was supported by National Science Foundation grant ATM-9531094 and NASA grant NAGW-4594. The Freja project is supported by the Swedish National Space Board (SNSB) and by the Deutsche Agentur für Raumfahrtangelegenheiten (DARA). The Freja satellite is managed and operated by the Swedish Space Corporation under contract from the Swedish National Space Board. We especially thank the Freja low-frequency F4 wave team. We also gratefully acknowledge informative and useful discussions with P. Schuck, P. Kintner, B. Lysak and B. Lotko.

The Editor thanks C. J. Pollock and another referee for their assistance in evaluating this paper.

References

André, M., P. Norqvist, A. Vaivads, L. Eliasson, O. Norberg, A. I. Eriksson, and B. Holback, Transverse ion energization and wave emissions observed by the Freja satellite, *Geophys. Res. Lett.*, *21*, 1915, 1994.

Bellan, P. M., Alfvén 'resonance' reconsidered: Exact equations for wave propagation across a cold inhomogenous plasma, *Phys. Plasmas*, *1*, 3523, 1994.

Bonnell, J., P. Kintner, J.-E. Wahlund, K. Lynch, and R. Arnoldy, Interferometric determination of broadband ELF wave phase velocity within a region of transverse auroral ion acceleration, *Geophys. Res. Lett.*, *23*, 3297, 1996.

Chen, F. F., *Introduction to plasma physics and controlled fusion*, vol. 1, Plenum, New York, 1984.

Crew, G. B., T. Chang, J. M. Retterer, W. K. Peterson, D. A. Gurnett, and R. L. Huff, Ion cyclotron resonance heated conics: Theory and observations, *J. Geophys. Res.*, *95*, 3959, 1990.

Eliasson, L., et al., Freja observations of heating and precipitation of positive ions, *Geophys. Res. Lett.*, *21*, 1911, 1994.

Erlandson, R. E., L. J. Zanetti, M. H. Acuña, A. I. Eriksson, L. Eliasson, M. H. Boehm, and L. G. Blomberg, Freja observations of electromagnetic ion cyclotron ELF waves and transverse oxygen ion acceleration on auroral field lines, *Geophys. Res. Lett.*, *21*, 1855, 1994.

Gekelman, W., D. Leneman, J. Maggs, and S. Vincena, Experimental observation of Alfvén wave cones, *Phys. Plasmas*, *1*, 3775, 1994.

Gekelman, W., S. Vincena, D. Leneman, and J. Maggs, Laboratory experiments on shear Alfvén waves and their relationship to space plasmas, *J. Geophys. Res.*, *102*, 7225, 1997.

Hui, C.-H., and C. E. Seyler, Electron acceleration by Alfvén waves in the magnetosphere, *J. Geophys. Res.*, *97*, 3953, 1992.

Ichimaru, S., *Basic Principles of Plasma Physics: A Statistical Approach*, Addison-Wesley, Redwood City, Calif., 1973.

Kintner, P. M., J. Vago, S. Chesney, R. L. Arnoldy, K. A. Lynch, C. J. Pollock, and T. E. Moore, Localized lower hybrid acceleration of ionospheric plasma, *Phys. Rev. Lett.*, *68*, 2448, 1992.

Kintner, P. M., J. Bonnell, R. Arnoldy, K. Lynch, C. Pollock, and T. Moore, SCIFER: transverse ion acceleration and plasma waves, *Geophys. Res. Lett.*, *23*, 1873, 1996.

Knudsen, D. J., and J.-E. Wahlund, Core ion flux bursts within solitary kinetic Alfvén waves, *J. Geophys. Res.*, *in press*, 1997.

Louarn, P., J.-E. Wahlund, T. Chust, H. de Feraudy, A. Roux, B. Holback, P. O. Dovner, A. I. Eriksson, and G. Holmgren, Observations of kinetic Alfvén waves by the FREJA spacecraft, *Geophys. Res. Lett.*, *21*(17), 1847, 1994.

Lynch, K. A., R. L. Arnoldy, P. M. Kintner, and J. Bonnell, The AMICIST auroral sounding rocket: a comparison of transverse ion acceleration mechanisms, *Geophys. Res. Lett.*, *23*, 3293, 1996.

Lysak, R. L., Feedback instability of the ionospheric resonant cavity, *J. Geophys. Res.*, *96*, 1553, 1991.

Lysak, R. L., Comment on "Theory of nearly perpendicular plasma waves and comparison to Freja satellite measurements," by C. E. Seyler and J.-E. Wahlund, *J. Geophys. Res.*, *current issue*, 1997.

Lysak, R. L., and W. Lotko, On the kinetic dispersion relation for shear Alfvén waves, *J. Geophys. Res.*, *101*(A3), 5085, 1996.

Marklund, G., L. Blomberg, C.-G. Falthammar, and P.-A. Lindqvist, On intense diverging electric fields associated with black aurora, *Geophys. Res. Lett.*, *21*, 1859–1994.

Morales, G. J., R. S. Lortisch, and J. E. Maggs, Structure of Alfvén waves at the skin-depth scale, *Phys. Plasmas*, *1*, 3765, 1994.

Norqvist, P., M. André, L. Eliasson, A. I. Eriksson, L. Blomberg, H. Lür, and J. H. Clemmons, Ion cyclotron heating in the dayside magnetosphere, *J. Geophys. Res.*, *101*(A6), 13179, 1996.

Seyler, C. E., A mathematical model of the structure and evolution of small-scale discrete auroral arcs, *J. Geophys. Res.*, *95*, 17199, 1990.

Seyler, C. E., and J.-E. Wahlund, Theory of nearly perpendicular electrostatic plasma waves and comparison to Freja satellite observations, *J. Geophys. Res.*, *101*(A10), 21795, 1996.

Seyler, C. E., J.-E. Wahlund, and B. Holback, Theory and simulation of low-frequency plasma waves and comparison to Freja satellite observations, *J. Geophys. Res.*, *100*, 21453, 1995.

Stasiewicz, K., G. Gustafsson, G. Marklund, P.-A. Lindqvist, J. Clemmons, and L. Zanetti, Cavity resonators and Alfvén resonance cones observed on Freja, *J. Geophys. Res.*, *102*, 2565, 1997.

Stringer, T. E., Low-frequency waves in an unbounded plasma, *J. Nucl. Energy C*, *5*, 89, 1963.

Swanson, D. G., *Plasma Waves*, Academic Press, San Diego, Calif., 1989.

Temerin, M., and R. L. Lysak, Electromagnetic ion cyclotron mode (ELF) waves generated by auroral electron precipitation, *J. Geophys. Res.*, *89*, 2849, 1984.

Temerin, M., J. McFadden, M. Boehm, C. W. Carlson, and W. Lotko, Production of flickering aurora and field-aligned electron flux by electromagnetic ion cyclotron waves, *J. Geophys. Res.*, *91*, 5769, 1986.

Trakhtengerts, V. Y., and A. Y. Feldstein, Quiet auroral arcs: Ionospheric effect of magnetospheric convection stratification, *Planet. Space Sci.*, *32*, 127, 1984.

Volwerk, M., P. Louarn, T. Chust, A. Roux, H. de Feraudy, and B. Holback, Solitary kinetic Alfvén waves: A study of the Poynting flux, *J. Geophys. Res.*, *101*, 13335, 1996.

Wahlund, J.-E., P. Louarn, T. Chust, H. de Feraudy, A. Roux, B. Holback, P.-O. Dovner, and G. Holmgren, On ion acoustic turbulence and the nonlinear evolution of kinetic Alfvén waves in the aurora, *Geophys. Res. Lett.*, *21*, 1831, 1994.

Wahlund, J.-E., et al., Broadband ELF plasma emission during auroral energization, 1, slow ion acoustic waves, *J. Geophys. Res.*, in press, 1997.

J. Bonnell, NIS-1 Atmospheric and Space Sciences, Mail Stop D466, Los Alamos National Laboratory, Los Alamos, NM 87545. (e-mail: jbonnell@lanl.gov)

A. E. Clark and C. E. Seyler, School of Electrical Engineering, Cornell University, Ithaca, NY 14853-7501. (e-mail: aclark@ee.cornell.edu; seyler@ee.cornell.edu)

J.- E. Wahlund, Swedish Institute of Space Physics (IRF), S-981 28 Kiruna, Sweden. (email: jwe@irfu.se)

(Received March 14, 1997; revised June 19, 1997; accepted August 7, 1997.)